NGR 05-002-294

CALIFORNIA INSTITUTE OF TECHNOLOGY

BIG BEAR SOLAR OBSERVATORY

HALE OBSERVATORIES

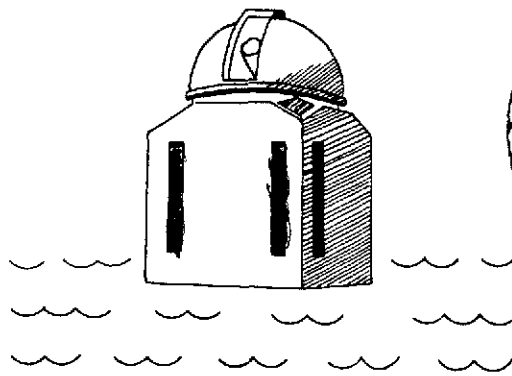

X-RAY BURSTS FROM SOLAR FLARES BEHIND THE LIMB

by

J.-René Roy *

and

Dayton W. Datlowe **

BIG BEAR SOLAR OBSERVATORY, HALE OBSERVATORIES

CARNEGIE INSTITUTION OF WASHINGTON

CALIFORNIA INSTITUTE OF TECHNOLOGY

BBSO # 0143

* Present address: The Astronomical Institute at Utrecht
Beneluxlaan 21, Utrecht, The Netherlands.

** Department of Physics, University of California, San Diego
La Jolla, California, U.S.A.

ABSTRACT

From the UCSD OSO-7 X-ray experiment data, we have identified 54 X-ray bursts with 5.1-6.6 keV flux greater than 10^3 photons $cm^{-2}sec^{-1}keV^{-1}$ which were not accompanied by visible Hα flare on the solar disk. By studying OSO-5 X-ray spectroheliograms, Hα activity at the limb and the emergence and disappearance of sunspot groups at the limb, we found 17 active centers as likely seats of the X-ray bursts beyond the limb. We present the analysis of 37 X-ray bursts and their physical parameters. We compare our results with those published by Datlowe et al. (1974 a and b) for disk events.

The distributions of maximum temperature, maximum emission measure, and characteristic cooling time of the over-the-limb events do not significantly differ from those of disk events. We show that of conduction and radiation, the former is the dominant cooling mechanism for the hot flare plasma. Since the disk and over-the-limb bursts are similar, we conclude that the scale height for X-ray emission in the 5-10 keV range is large and is consistent with that of Catalano and Van Allen (1973), for primarily 1-3 keV emission, 11,000 km.

Twenty-five or about 2/3 of the over-the-limb events had a nonthermal component. The distribution of peak 20 keV flux is not significantly different from that of disk events. However, the spectral index at the time of maximum flux is significantly different for events over the limb and for

events near the center of the disk; the spectral index for over-the-limb events is larger by about $\Delta\gamma = 3/4$. If hard X-ray emission came only from localized sources low in the chromosphere we would expect that hard X-ray emission would be occulted over the limb; on the contrary, the observations show that the fraction of soft X-ray bursts which have a nonthermal component is the same on and off of the disk. Thus hard X-ray emission over extended regions is indicated.

1. INTRODUCTION

Solar X-ray bursts contain emission of two general types. In the range below 10 keV, thermal emission from a plasma assumed to have a Maxwellian electron distribution with a temperature of the order of 10^7 K (Culhane and Philips, 1969) dominates the spectrum. At higher energies, the spectrum is conventionally represented as a power law of the form $F(h\nu) = A\ (h\nu)^{-\gamma}$ where $F(h\nu)$ is the flux in photons $cm^{-2} sec^{-1} keV^{-1}$ and γ the spectral index.

At energies greater than a few keV, various experiments have recorded the time profile of the X-ray flux from the entire visible solar disk. Observing solar X-ray bursts from various locations in space opens multiple possibilities for studying geometrical and physical properties of the coronal plasma. The technique of observing a burst with two different spacecraft at different heliocentric longitudes has been applied successfully by Catalano and Van Allen (1973), who determined the scale height of the soft X-ray emission in the 2-12 Å is 1.1×10^4 km. Using lunar occultation of an X-ray burst, Kreplin and Taylor (1971) determined that the spatial extent of X-ray emission in the 1-8Å range to be 140,000km. Imaging experiments have also been flown (Vaiana et al. 1973 a and b) to measure the sizes of soft X-ray emitting regions. For hard X-rays comparable experiments have not been possible.

Wood et al. (1972) observed EUV radiation correlated well in time with nonthermal X-ray emission, and concluded that this emission was due to heating by collision losses of the X-ray emitting electrons. The spectral lines involved were characteristic of the chromosphere. They concluded that the chromosphere was heated directly by nonthermal electrons. In this case the ambient density is large enough that electrons are expected to lose all of their energy to collisions (Hudson, 1973), so that the thick-target approximation is applicable. Vorpahl (1974) has given a model in which electrons are accelerated in arch systems at heights of ~5000 km; these electrons move down magnetic flux tubes, producing correlated X-ray, microwave, and Hα bright-point emission. Kane and Donnelley (1971) and Kane (1974) have proposed a similar model, except that electrons with $E \tilde{} 20$ keV escape to the corona, where they emit X-rays by the thin-target process. In all of these cases there is a thick-target X-ray component at low altitudes; this should be occulted by the solar limb for any flare more than 7° behind the limb, corresponding to a minimum visible height of 5000 km.

X-ray emission from high in the corona is also possible. Frost and Dennis (1971) reported hard X-ray emission from the flare of March 30, 1969, which was well behind the limb. Lin (1972) has reported the observation of solar electrons in

interplanetary space with a spectrum extending down to 6 keV; these electrons must have been accelerated in the lower corona or above in order to reach the earth. Datlowe and Lin (1974) have reported a correlated observation of X-rays, type III bursts, and interplanetary electrons; comparison of the electron and X-ray spectra indicates that thin-target emission was the origin of the X-ray burst. X-ray emission of this type, extending far into the corona, should be occulted only slowly with increasing solar longitude.

There exists one measurement of the spatial extent of a hard X-ray emitting region (Takakura et al. 1971). The observational technique consisted of a balloon-borne modulation collimator for X-rays in the energy range 20-60 keV. The size of the hard X-ray source was estimated to be about one minute of arc (50,000km), but no estimate of the height of the emission came from this data. Balloon borne observations can be expected to make only very few observations of this type; however, satellite borne hard X-ray imaging experiments of this type could bring in significant new information on hard X-ray emission processes. Such observations represent the outstanding observational problem in hard X-rays at the present time. However, hard X-ray imaging systems are not to be ready before the next solar maximum; thus one must use another method such as limb occultation of a large group of flares to learn about the physical extent and height dependence of the spectrum of hard X-rays.

Occultation allows us to determine the respective heights of soft and hard X-rays. If hard X-rays arise from very high temperature plasmas as proposed by Chubb (1970) and Brown (1973), occultation may put some limit on the dimensions of the hard X-ray flare and serve as a probe for the temperature structure of the coronal cloud. If on the other hand, hard X-rays are produced by electrons releasing their energy through non-thermal bremsstrahlung (Brown, 1971), occultation can help to pinpoint the site of X-ray emission.

Here we present the results of a search for behind the limb X-ray bursts using data from the UCSD experiment on OSO-7. The UCSD solar X-ray experiment uses a two-detector system to cover energy ranges which correspond with X-rays of thermal and non-thermal origin in solar bursts: a proportional counter which has eight energy channels between 2-15 keV and scintillator which has nine logarithmically spaced channels between 10-320 keV. Harrington et al. (1972) and McKenzie et al. (1973) give more details on the experiment.

2. DATA SELECTION

From the rich supply of observations reported by Vaiana et al. (1973 a and b), it is evident that the spatial distribution

or geometry of the X-ray sun is determined by the coronal magnetic fields. Rust and Roy (1971) and Roy (1972) have demonstrated that coronal magnetic fields above active regions are closely matched by field lines computed from a potential field calculated from measured photospheric fields; most structures related to flare activity are expected to show extent in height of the same order as the size of active regions, e.g. 10^5 km. Accordingly, one should expect the X-ray emission to be visible from bursts located as far as 30° behind the limb, i.e. more than two days before or after limb passage of the associated active group.

Before searching for bursts originating from behind-the-limb active regions, we established a threshold of soft X-ray flux above which the absence of reported Hα flare would suggest a likely candidate for a limb occulted flare. McKenzie (1973, unpublished) found that 76% of 601 OSO-7 X-ray bursts above 10^3 photons cm^{-2} sec^{-1} keV^{-1} had an associated Hα flare reported in Solar Geophysical Data (SGD). Datlowe et al. (1974a) found a similar percentage of identical flares in 197 bursts also from the OSO-7 instrument. Reduced visibility near the limb and lack of visibility behind the limb can account for soft X-ray bursts in the absence of an Hα flare; the largest bursts on the disk remain associated with easily detectable

Hα emission and are less sensitive to longitude fall-off effects. If the remaining 24% of the bursts are from flares behind the limb and if we assume that flares occur uniformly all around the sun, it is required that big soft X-ray bursts stay visible as far as 28° over the limb; this would mean that the emission needs to extend as far as 10^5 km. Therefore, we choose the 5.1-6.6 keV OSO-7 proportional counter channel and establish the threshold flux at 10^3 photons cm^{-2} sec^{-1} keV^{-1}.

Although SGD is incomplete in reporting small flares or events near the limb, small X-ray bursts of the order of 10^2 photons cm^{-2} sec^{-1} keV^{-1} can be associated with Hα events on high resolution filtergrams of the whole sun (Figure 1). For the OSO-7 observing period, soft X-ray bursts with 5.1-6.6 keV fluxes greater than 10^3 photons cm^{-2} sec^{-1} keV^{-1} were observed in association with 64 Hα disk flares recorded on filtergrams taken by the 8.6-in. vacuum telescope at Big Bear Solar Observatory and nine more events recorded with the Tel Aviv photoheliograph. Of these 73 events, five (7%) were not recorded by SGD. Therefore, a selection of large X-ray bursts without Hα flare reported in SGD would be contaminated by missed disk events to a small degree. However, because of our selective procedure, this 7% represents an upper limit. A burst with no SGD reported flare is not the sole criterion for beyond-the-limb candidacy; three more criteria described in the following are used to ensure the right identification.

After initially identifying 115 bursts with no Hα flare

with 5.1-6.6 keV flux above threshold, we investigated their possible association with the presence of a large active region near east or west limb within a few days of the burst occurrence. Early in our search, a link between chains of strong bursts with flaring activity behind the limb was suggested by the obvious clustering in time of the bursts, with each family occuring within two days of limb passage of large sunspot groups. We present six families of such bursts in Table I with their associated candidate regions. This clustering proved very helpful in pinpointing candidate regions.

Furthermore, to ensure the proper identification, we relied on various data such as chromospheric activity, like surges or eruptive prominences, appearing above the limb; in most cases, such activity was seen to occur continuously prior to and after the bursts without showing close direct association with the bursts. Study of Tel Aviv and Big Bear Solar Observatory Hα films provided in this way reliable indications of activity beyond the limb.

The most helpful observations for identifying activity behind the limb and discriminating between east and west limbs as its seat, were the soft X-ray contour maps with spatial resolution of 1.6 arc min obtained by the University College of London and Leicester University X-ray experiment on OSO-5. The maps reproduced in SGD are from one or two orbits of "quick-look" data and give a solar image at 9.1-10.5 Å. The maps are from non-flare periods and display in a striking way the hot coronal

components of active regions. The X-ray enhancement appears or disappears well before or after east or west limb passage of a group. (see Appendix I)

After selecting 17 candidate regions, we determined the location of the groups over the limb. The position of each candidate was plotted as a function of time from Mt. Wilson sunspot drawings and McMath plage data for four to seven days following or preceding limb passage; these positions represent roughly the center of the groups or plages. This position vs time relation was extrapolated beyond 90° such as in Figure 3 which applies to Mt Wilson sunspot group 18839. For most cases there is good agreement with Newton and Nunn (1951) relationship for large recurrent sunspots,

$$\omega = 14.38 - 2.77 \sin^2\phi \quad \text{deg day}^{-1}, \qquad (1)$$

where ϕ is the region latitude. In some cases, the groups display a slower rotation rate than predicted by (1).

Once the positions of the active regions are established, the minimum height above which X-ray emission becomes visible can be calculated following a few assumptions: first the X-ray emission originates in the corona radially above the chromospheric flare; second we locate the would-be flare near the active region center; finally, we calculate the minimum height by neglecting the effect of the latitude. The error introduced by the last assumption is small in comparison with uncertainties in the flare position and sunspot motions or changes. The

height above which X-ray emission is observed can be expressed as

$$h \gtrsim 6.97 \times 10^5 \quad \frac{(1 - \sin \theta)}{\sin \theta} \quad \text{km}, \qquad (2)$$

where θ is the longitude in degrees from the central meridian. Table A (Appendix II) gives 54 strong X-ray bursts accompanied by no Hα flare. The bursts originate from 17 candidate active regions; their extrapolated positions and the burst minimum visible heights are given in the last two columns. The events at $\theta \lesssim 90°$ had no reported chromospheric flares; because of the procedure by which θ is defined, these events might have occurred slightly beyond the limb.

In addition to those events, we have selected a set of 37 non-thermal 'limb' bursts identified from SGD as coming from flares located between $60° \lesssim \theta \lesssim 90°$. As a reference for comparison to these, we used the same set of 59 non-thermal events at $0 \lesssim \theta < 60°$ as used in Datlowe et al. (1974b), hereafter identified as 'center' events.

3. ANALYSIS OF THE X-RAY BURSTS

The procedure for analyzing solar X-ray bursts in the energy ranges of 5-15 keV and 10-100 keV from OSO-7 data has been previously described in detail by McKenzie et al. (1973) and Datlowe et al. (1974 a and b). Datlowe et al. (1974 a and b) also give the available range of the thermal emission and non-thermal spectrum parameters for the OSO-7 detector. We give a summary of the method in Appendix III.

I. THE PARAMETERS OF THE THERMAL X-RAY EMISSION

i) TEMPERATURE AND EMISSION MEASURE BEHAVIOR

The spectra of 37 of the total 54 over-the-limb X-ray bursts were analyzed. The maximum temperature T_{max} distribution of the thermal bursts behaves like the one of bursts accompanying flares on the disk (Figure 4a). The median T_{max} is identical, i.e. 17×10^6 K. The distribution of T_{max} for the three sets of events do not exhibit statistically significant differences. The behavior of T_{max} versus distance beyond the limb of the candidate sunspot group (giving dependence on minimum visible height of the burst) reveal no definite trend (Figure 4c).

EM_{max} is the maximum emission measure under the constraint that the temperature must have been above 10^7 K (see Figure 1 of Datlowe et al. 1974 a). The distribution of EM_{max} does not differ in a statistically significant way from the same distribution of center events. The median value for EM_{max} is

50×10^{47} cm^{-3} for over-the-limb bursts; this is higher than 30×10^{47} cm^{-3} for bursts accompanying disk subflares, but similar to EM_{max} of bursts associated with Imp 1 flares on the disk. This would indicate that over-the-limb bursts originate from bigger flares. EM_{max} is plotted as a function of minimum visible height of the burst in Figure 4d; again the data is insufficient to indicate any definite trend.

ii) THE COOLING PROPERTIES OF THE THERMAL X-RAY BURSTS

We have studied the thermal evolution of the events by defining a convenient form for the characteristic cooling time, τ,

$$(\tau)^{-1} \approx \frac{1}{T}\frac{dT}{dt} . \qquad (3)$$

We compared the cooling times of 33 over-the-limb events (Figure 5) with those of 77 events analyzed by Datlowe et al. (1974a). Although the median cooling time of 800 sec for over-the-limb events is larger than the 600 sec typical of disk bursts, the distributions do not differ significantly (Table II).

The two dominant cooling mechanisms are radiation and conduction, which have a different dependence of cooling rate with temperature. The characteristic cooling time by radiation is expressed in a convenient form as

$$t_R = \frac{3\ kT}{n_e\ L_R\ (n_e, T)} \sim \frac{(kT)^{1/2}}{n_e} , \qquad (4)$$

where L_R, a weak function of the temperature around 10^7 K, is the cooling rate coefficient, ergs cm^{+3} sec^{-1}. In our computation, we have used values for L_R from Culhane et al. (1970) who take into account line and continuum processes. Densities of the X-ray emitting coronal plasma may be calculated approximately from the values of the emission measure $n_e^2 V$ and from estimate of flare volumes deduced from the size of the chromospheric Hα flare. Those densities are found to vary only a little, being of the order of a few times 10^{10} cm^{-3} (Hudson and Okhi, 1972; Neupert et al., 1974; Rust and Roy, 1974). For these typical flare plasma densities, the characteristic cooling times are $\tau \approx 10^4$ sec. Moreover, if radiative cooling dominates, we expect a positive correlation between the cooling time and the peak temperature.

For conduction cooling, lack of electron mobility across magnetic fieldlines converts the problem to one dimension. The relevant length is the dimension ℓ along the magnetic field lines threading the flare volume. The characteristic cooling time by conduction may be expressed in a similar way by

$$t_C = \frac{3\, n_e\, k\ell^2}{\kappa} \quad \text{sec} \qquad (5)$$

where

$$\kappa = 1.844 \times 10^{-5} \frac{T^{5/2}}{\ln\Lambda} \quad \text{ergs sec}^{-1}\text{cm}^{-1}\text{K}^{-1} \qquad (6)$$

and is the coefficient of thermal conductivity along the magnetic field. In Λ, the Coulomb logarithm, is about 20

for the range of temperatures and densities we are concerned with. ℓ is the characteristic dimension of the conduction cooling path. So the temperature dependence of conduction cooling times goes as

$$T \sim (\alpha\tau)^{-2/5} \qquad (7)$$

where α is a function of n_e and ℓ^2. This predicts a coefficient of correlation between the cooling time and T_{max} which is negative. Unlike radiative cooling, conductive cooling is sensitive to the geometry assumed, and a priori estimates cannot be made as to conductive cooling times.

The distribution of characteristic cooling times of 33 over-the-limb events, shown in Figure 5, is an order of magnitude less than predicted by radiative cooling

For 50 events of 122 in Datlowe et al. (1974b), the correlation between T_{max} and has been determined; the correlation coefficient is -0.6. The corresponding coefficient of correlation for 39 limb and over-the-limb events is -0.4. How good the correlation is remains uncertain, but we are confident that its sign is negative. We have considered instrumental biases and concluded that the origin of the correlation is not instrumental. Thus the observational evidence favors conduction as the dominant cooling mechanism over radiation.

Figure 6 exhibits a power law temperature decay of the form

$$T = T_o \quad (t - t_o)^{-\mu} \qquad (8)$$

where $\mu = 0.2$. An exponent value of $\mu = 0.4$ is expected from conductive cooling. We have identified five more over-the-limb events with a power law cooling. In each case an exponential $e^{-t/\tau}$ does not fit. The typical $\mu = 0.2$.

II. HARD X-RAYS FROM OVER-THE-LIMB EVENTS

i) CORRELATION WITH NON-THERMAL EVENTS

Of the 37 analyzed bursts with 5.1-6.6 keV flux greater than 10^3 photons cm^{-2} s^{-1} keV^{-1}, 25 bursts or about 2/3, have a non-thermal component. This ratio is the same as found by Datlowe et al. (1974 a and b) for similar size thermal bursts accompanying flares on the disk. The fact that such a ratio is the same for partially occulted bursts suggests that non-thermal X-ray radiation originates at least as high in the corona as the soft X-ray thermal radiation.

ii) DURATION AND FULL-WIDTH AT HALF MAXIMUM OF NON-THERMAL EVENTS

To compare the time histories of non-thermal events, we have studied the duration and the full-width at half maximum (FWHM) of the 20 keV hard X-ray flux. "Duration" as used here means the time interval over which the flux is above the threshold for analysis, A = 0.1 photons cm^{-2} $sec^{-1}keV^{-1}$. "FWHM" is similar, except that the threshold is replaced by 1/2 A_m, A_m being the 20 keV peak flux.

As shown in Table II, the median values of duration and FWHM are the same for limb and center events. The median duration and median FWHM for over-the-limb events are larger by 50% and 75% respectively than those of limb and center events. The distribution of durations for over-the-limb is not statistically different from the limb and center events

distributions. The distribution of FWHM of over-the-limb events is statistically different with a probability of the distribution occurring at random of 3×10^{-3} .

iii) DISTRIBUTION OF THE PEAK FLUX AND SPECTRAL INDEX OF HARD X-RAYS FROM OVER THE LIMB

The median value of the 20 keV peak flux is $A_m = 0.84$ photons cm^{-2} sec^{-1} keV^{-1} for over-the-limb bursts; this is about the same as found by Datlowe et al. (1974b) for 122 disk bursts. The distribution is also identical for the limb events with $A_m = 0.79$ (Table II). The distributions are not statistically different (Figure 7).

As a representative value of the spectral index, we use the value at the time of maximum 20 keV flux, γ_m. Figure 8b shows the distribution of this quantity for the limb and for the over-the-limb events; the same distribution for the center events is shown in Figure 8a. To determine the probability that the distribution in 8b is a random sample of the distribution shown in 8a, we use the Kolmogorov-Smirnov test (Brunk, 1960). The result is that the probability that the 25 over-the-limb spectral indices are a random sample of the distribution 8a is 5×10^{-3}; for the 37 limb events, the corresponding probability is 5×10^{-3}; for the 62 events combined, it is 8×10^{-4}. We conclude that the difference in the distributions 8a and 8b is statistically significant. The spectra of events near and beyond the limb are steeper by about $\Delta\gamma = 3/4$.

4. CONCLUSIONS

Our first conclusion is that the thermal emission of limb occulted X-ray bursts does not differ from that of events near the center of the disk. This is consistent with the interpretation that the scale height of soft X-ray emission in the energy range 5-10 keV is similar to that found by Catalano and Van Allen, (1973), 11,000 km, for X-ray emission primarily in the range 1-3 keV. Alternatively, the occultation of the soft X-ray source in this sample of over-the-limb bursts was a small effect.

Within the context of whether the dominant cooling mechanism is radiation or conduction, these observations support conduction. First, the observed cooling times derived from the temperature histories of the over-the-limb and limb bursts are too small to be explained by radiative cooling. Secondly, we observe an anticorrelation between the maximum temperature and the cooling time, which is expected on the basis of conduction cooling and not from radiation. Thirdly, for a static flare plasma with impulsive heat injection, the decay of the temperature would be described by a power law $T \sim t^{-\mu}$, where $\mu=.4$. In those five cases where the temperature decay was described unambiguously by a power law, the observed exponent $\mu=.2$, in reasonable agreement with conduction.

However, it should be pointed out that the problem as formulated here is not strictly applicable to the solar plasma. In this formulation we infer from a decrease in temperature that heat is flowing out of the flare plasma. However, during the growth phase of the flare plasma, heat is rapidly being added in the form of new hot material, even though the temperature is declining. In particular, if the heat in the flare plasma is represented by Q, then

$$\frac{dQ}{dt} = \frac{d}{dt}(3N_e kT) = 3kT\frac{dN_e}{dt} + 3N_e k\frac{dT}{dt} \qquad (9)$$

and during the growth phase of the flare plasma, the term dN_e/dt clearly dominates the heat flow (Datlowe et al., 1974a). Curiously the temperature evolution is largely independent of the growth of the emission measure; the rate of change of temperature is apparently unaffected by the presence or absence of the convective heat input (dN/dt) term. A model which would take these features of the heat flow into account would be considerably more sophisticated than is implied by the two alternatives, conduction and radiation. Nonetheless, within the limited framework in which the question of conduction versus radiation is meaningful, the present data strongly favor conduction as the dominant cooling mechanism.

The spectral index of the hard X-ray burst at maximum flux γ_m, is steeper by about $\Delta\gamma = 3/4$. As compared with the earlier paper (Datlowe et al., 1974 b) in which this effect was

reported, the statistical significance of the result has been improved by about a factor of 10 due to an increase in the number of events with $\theta>60°$, from 27 to 62. This is not however an independent confirmation of the earlier result, since all the events of the earlier paper are included in the present sample. We are confident that this is a statistically significant ($p\simeq 10^{-3}$) experimental result and that it is not the result of an instrumental bias.

The most important result of the over-the-limb burst characteristics is that the fraction of the bursts which have a non-thermal component is 2/3, exactly the same as found for the 122 X-ray bursts studied in Datlowe et al. (1974b). What is more, of the eight bursts with expected locations with θ greater than 100°, corresponding to minimum visible heights from 10^4 to 10^5km, five exhibit a detectable non-thermal component.

Thick-target models of X-ray emission assume that the X-ray emitting region is low in the chromosphere. On this basis, we would expect that the hard X-ray source would be rapidly occulted with increasing longitude of the burst location. What we have observed is just the contrary. One possibility is that X-ray emission extends to heights between 10^4 and 10^5 km; in this case the density of the solar atmosphere is sufficiently low that escape loss may dominate collision loss and we would expect thin-target emission. A

second possibility is that electrons accelerated in the flare travel over long distances via magnetic arches, reentering the high density regions far from their acceleration site. In this case we would not see occultation of the hard X-ray source even though the electrons may stop at low altitudes. In either case, localized emission from chromospheric bright points is not consistent with the emission which we see from beyond the limb.

We note that our observational result, that hard X-ray emission takes place on height scales of the order of 10^4-10^5 km, is consistent with the size scales implied by the previous observational data of Catalano and Van Allen (1973), Takakura et al. (1971), and Kreplin and Taylor (1970). The result is however very different from what we would have expected on the basis of the correlation of hard X-ray bursts with EUV and Hα bright point observations.

A possible explanation of the spectral difference between center and over-the-limb bursts is that all bursts exhibit both kinds of emission; in the center events thick-target emission dominates, but for the limb events the thick target source is occulted and thin-target emission dominates (H. Hudson, priv. comm.). The difference between the spectral distribution is consistent with this interpretation although the magnitude of the difference, $\Delta\gamma = 3/4$ is too small. However

there are difficulties with this interpretation. First, we are at a loss to know how the thick-target source can be occulted or absorbed in the case of the bursts from $60 \lesssim \theta \lesssim 90°$, and yet their spectrum is like those of the over-the-limb events. Secondly, we would expect that when the low-lying hard X-ray source-- which dominates the emission on the disk -- is occulted, then for a given burst, the emission measure and the hard X-ray flux observed from an over-the-limb burst would be substantially reduced. However, this is not observed (see table II).

In conclusion, these occultation measurements indicate that hard X-ray emission takes place from extended regions in the solar atmosphere.

ACKNOWLEDGEMENTS

Our thanks go to H. S. Hudson, M. Elcan of University of California, San Diego and to R. L. Moore, Sou-Yang Liu, H. Zirin of the California Institute of Technology for their enlightening discussions and helpful comments. We are grateful to Larry Bergo of UCSD and Frances Tang of Caltech for their careful work in the various stages of the data analysis. W. M. Glencross of University College of London kindly provided some OSO-5 X-ray spectroheliograms.

One of us (J.R.R.) acknowledges support from US Air Force contract F19628-73-C-0085 and NASA Grant NGR 05 002 294. The OSO-7 X-ray analysis is supported by NASA contract NAS-5-11081.

FIGURE CAPTIONS

Figure 1. X-ray bursts recorded by the OSO-7 UCSD experiment and simultaneous whole disk Hα filtergrams showing the accompanying Hα flares taken by the 8.6-in. vacuum telescope at Big Bear Solar Observatory; the fluxes of these two events differ by almost three orders of magnitude. Subflares with 5.1-6.6 keV flux as low as 100 photons $cm^{-2}s^{-1}$ keV^{-1} can be identified on such filtergrams.

Figure 2. Powerful X-ray bursts without recorded Hα activity on filtergrams taken by the 8.6-in. vacuum telescope at Big Bear Solar Observatory.

Figure 3. Position of active center Mt Wilson 18839-McMath 11895 on the solar disk and extrapolated beyond east limb; the times and positions of its associated occulted X-ray bursts are also shown.

Figure 4. (a) Distribution of maximum temperature for the individual over-the-limb bursts.

(b) Distribution of maximum emission measure for the individual over-the-limb bursts.

(c) Maximum temperature as a function of minimum visible height for each occulted burst.

(d) Maximum emission measure as a function of minimum visible height for over-the-limb bursts.

Figure 5. Distribution of characteristic cooling times for 33 over-the-limb events. τ is defined in the text.

Figure 6. An example of a burst for which the temperature decay fits a power law. This event occurred on Feb. 8, 1972.

Figure 7. Distribution of peak 20 keV flux for individual over-the-limb events.

Figure 8. (a) Distribution of the frequency of occurrence of the spectral indices at peak 20 keV flux for 59 center events.

(b) Same distribution for 37 limb events (hatched) and for 25 over-the-limb events (black).

FIGURE CAPTIONS

Figure A. OSO-5 9.1-10.5 Å X-ray contour map on 22-23 May 1972. Contour intensities are in units of 10^{-6} ergs cm^{-2} sec^{-1}. The strong enhancement near the east limb is associated with flare activity occuring in McMath region 11895 (Mt Wilson 18935) at East 102°; the group is to rotate on the disk late on May 23 or early on May 24. (University College of London and Leicester University)

Figure B. White-light photograph of the solar disk around 1630 UT on May 25, 1972. Mt Wilson sunspot group 18935 which appeared at the east limb 1 1/2 day earlier is pointed out.

REFERENCES

Brown, J. C.: 1971, Solar Phys. 18, 489.

Brown, J. C.: 1973, in G. Newkirk (ed.) "Coronal Disturbances" IAU Symp. #57, in press.

Brunk, H. D.: 1960, An Introduction to Mathematical Statistics, Ginn and Co., Boston, p. 351.

Catalano, C. P. and Van Allen, J. A.: 1973, Astrophys. J. 185, 335.

Chubb, T. A.: 1972, in Dyer (ed.) "Solar Terrestrial Physics I 1970", D. Reidel Pub. Co. Part I, 99.

Culhane, J. L. and Philips, K. J. H.: 1969, Solar Phys. 11, 117.

Culhane, J. L., Vesceky, J. F. and Philips, K. J. H.: 1970, Solar Phys. 15, 394.

Datlowe, D. W. and Lin, R. P.: 1973, Solar Phys. 32, 459.

Datlowe, D. W., Hudson, H. S. and Peterson, L. E.: 1974a, Solar Phys. 35, 193.

Datlowe, D. W., Elcan, M. and Hudson, H. S.: 1974b, submitted to Solar Physics.

Frost, K. J. and Dennis, B. R.: 1971, Astrophys. J. 165, 655.

Harrington, T. M., Maloy, J. O., McKenzie, D. L. and Peterson L. E.: 1972, IEEE Trans. Nuc. Sci., NS-19, 596.

Hudson, H. S. and Okhi, K.: 1972, Solar Phys. 23, 125.

Hudson, H. S.: 1974, in Ramaty and Stone (ed.) "High Energy Phenomena on the Sun", Symposium Sept. 28-30, 1972, 207.

Kane, S. R.: 1973, in G. Newkirk (ed.), "Coronal Disturbances" IAU Symp. #57, in press.

Kane, S. R. and Anderson, K. A.: 1970, Astrophys. J. 162, 1003.

Kane, S. R. and Donnelley, R. F.: 1971 Astrophys. J. 164, 151.

Kreplin, R. W. and Taylor, R. G.: 1971, Solar Phys. 21, 452.

Lin, R. P.: 1974, in Ramaty and Stone (eds.), "High Energy Phenomena on the Sun" Symposium Sept. 28-30, 1972, 439.

McKenzie, D. L.: 1972, Astrophys. J. 175, 481.

McKenzie, D. L., Datlowe, D. W. and Peterson, L. E.: 1973, Solar Phys. 28, 175.

Neupert, W. M., Thomas, R. J. and Chapman, R. D.: 1974, Solar Phys. 34, 349.

Newton, H. W. and Nunn, M. L.: 1951, Monthly Notices Roy. Astron. Soc., 111, 413.

Roy, J.-R.: 1972, Solar Phys. 26, 418.

Rust, D. M. and Roy, J.-R.: 1971, in R. Howard (ed.) "Solar Magnetic Fields", IAU Symp. 43, 569.

Rust, D. M. and Roy, J.-R.: 1974, The late June 1972 "Cinof" Flares, AFCRL Research Report TR-74-0201.

Takakura, T., Ohki, K., Shibuya, N., Fujii, M., Matsuoka, M., Miyamoto, S., Nishimura, J., Oda, M., Ogawara, Y., and Ota, S.: 1971, Solar Phys. 16, 454.

Vaiana, G. S., Krieger, A. S. and Timothy, A. F.: 1973a, Solar Phys. 32, 81.

Vaiana, G. S., Davis, J. M., Giacconi, R., Krieger, A. S. Silk, J. K., Timothy, A. F. and Zombeck, M.: 1973b Astrophys. J. (Letters) 185, L47.

Vorpahl, J. A.: 1974, in Ramaty and Stone (eds.) "High Energy Phenomena on the Sun" Symposium Sept. 28-30, 1972, 222.

Wood, A. T. and Noyes, R. W.: 1972, Solar Phys. 24, 180.

APPENDIX I

The most helpful observations for identifying activity behind the limb and discriminating between east and west limbs as its seat, were the soft X-ray contour maps with spatial resolution of 1.6 arc min obtained by the University College of London and Leicester University X-ray experiment on OSO-5. The maps reproduced in SGD are from one or two orbits of "quick-look" data and give a solar image at 9.1-10.5 Å. The maps are generally from non-flare periods and display in a striking way the hot coronal components of active regions. The X-ray enhancement appears or disappears well before or after east or west limb passage of a group, typically one to two days. Such a map with contour intensities in units of 10^{-6} ergs $cm^{-2}sec^{-1}$ is shown in Figure A for May 22-23 1972; the strong X-ray source near the east limb was associated with McMath region 11895 (Mt. Wilson 18935) which produced seven X-ray bursts with fluxes greater than 10^3 photons $cm^{-2}sec^{-1}keV^{-1}$ with limb occulted Hα flares (Figure 3 in the text). Figure B shows a white light picture of the sun on May 25, 1972 (1630 UT) at Mount Wilson Observatory. McMath region 11895 is indicated by an arrow.

APPENDIX II

Table A gives 54 strong X-ray bursts (5.1-6.6 keV flux greater than 10^3 photons cm^{-2} sec^{-1} keV^{-1}) accompanied by no Hα flare. The bursts originate from 17 candidate active regions; their extrapolated positions and the burst minimum visible heights are given in the last two columns.

APPENDIX III

Computation of X-ray burst physical parameters

Table B lists the 37 X-ray bursts for which the thermal plasma and non-thermal electron distribution parameters were determined using the OSO-7 counting rate data. The procedure has been discussed in more details by McKenzie et al. (1973). We give the main points of the method.

The temperature T of the X-ray emitting plasma can be calculated by taking the ratio of the fluxes measured in the different channels. Knowing the flux at the satellite and the temperature of the plasma allows the calculation of the emission measure $\int_V n_e^2\, dV$ following Culhane et al. (1970):

$$N(E) = 4.4 \times 10^{-41} E^{-1.3} T^{0.2} \exp\left[\frac{-E}{kT}\right]\left[1-\left(\frac{E}{88.0}\right)^{0.33kT}\right]^{-1.0} \times \int_V n_e^2\, dV \quad \text{photons cm}^{-2}\text{sec}^{-1}\text{keV}^{-1} \text{ at earth distance,} \qquad \text{(i)}$$

where E is the photon energy in keV, T is the electron temperature in deg K and $\int n_e^2\, dV$ is the emission integral. T and $n_e^2 V$ are determined by the best fit to the pulse height distribution when folded through the proportional counter response including resolution spread. The several constraints on the dynamic range over which the analysis can be carried out have been discussed by Datlowe et al. (1974 a and b). Columns five and six of Table B give the maximum values of the temperature and emission measure for each event.

The spectrum above 10 keV consists of a power law of the form

$$F(h\nu) = A(h\nu)^{-\gamma} \qquad \text{(ii)}$$

where F ($h\nu$) is the flux in photons cm^{-2} $sec^{-1}keV^{-1}$ and γ the spectral index, plus an extrapolation of the thermal spectrum. Using T and n_e^2V previously determined, the event is classified as Hard (column four). The values of A and γ are determined by the best fit to the pulse height distribution when the spectrum is folded through the response of the scintillator.

The index γ_m in column eight is the value of γ at the time of peak non-thermal 20 keV flux. The value γ_{min} is less reliable and represents the smallest spectral index computed during the portion of the event which was analysed.

To determine the electron spectrum which produces the hard X-rays, one has to assume something about the way electrons dispose of their energy. In one case, the electrons rapidly transfer their energy to the medium through collisions or plasma wave-particle interactions; this is the so-called thick-target model. In the second case, called thin-target model, decay is dominated by the escape of suprathermal electrons to a region in the corona where density is low enough that bremsstrahlung does not occur at detectable levels.

Brown (1971) has shown that the thick-target power input in the form of kinetic energy of electrons above $E_c$keV, where

E_c is a low energy cut-off in the electron spectrum, is

$$P_{thick}(E_c,\gamma) = 4.29 \times 10^{24} A\gamma^2(\gamma-1)\, B(\gamma-1,3/2) \times E_c^{-(\gamma-1)} \text{ erg sec}^{-1}, \qquad \text{(iii)}$$

where $B(x,y)$ is the Beta function.

If escape dominates (thin-target), the X-ray spectrum arises from a population of electrons whose spectrum is nearly unchanged from the injection spectrum. The thin-target power is

$$P_{thin} = P_{thick}/\gamma \qquad \text{(iv)}$$

An average value for the spectral index $\bar{\gamma}$ may be defined over the inferred electron spectrum in the following way

$$\bar{\gamma} = \frac{\Sigma\, P_{thick}\ \Delta t}{\Sigma\, P_{thin}\ \Delta t} \qquad \text{(v)}$$

Table 1

Active regions with X-ray bursts behind the limb

Date of burst	Number of bursts	Candidate region		Limb passage		
		Mt Wilson	McMath	Limb	Date	Approximate time
31 Dec 71-1 Jan 72	6	18665	11656-57	West	31 Dec. 71	0000 UT
13 May 72	4	18834	11883	East	13 May 72	2000 UT
22-23 May 72	7	18834	11895	East	24 May 72	0000 UT
11-12 Aug. 72	6	18935	11976	West	11 Aug. 72	1000 UT
26-27 Aug. 72	4	18962	12011	East	26 Aug. 72	2200 UT
22-23 Oct. 72	7	19026	12044	East	23Oct. 72	0000 UT

TABLE II*

X-ray burst parameters

Location	Events	A_m**	Duration+ (sec)	FWHM (sec)	γ_m ++	$\bar{\gamma}$	τ (sec)	EM (cm^{-3})	T (10^6k)
Over limb	25	0.84	123	71	4.6	5.2	800	5×10^{48}	17.6
Limb	37	0.79	82	41	4.4	4.9	650	4×10^{48}	17.3
Center	59	0.90	92	31	3.8	4.3	570	3×10^{48}	17.7
All events+++	122	0.77	92	46	4.0	4.6	600	4×10^{48}	17.2

* Quantities listed here are median values.

** Peak 20 keV flux in photons cm^{-2} sec^{-1} keV^{-1}.

\+ Duration above the threshold of 0.1 photons cm^{-2} sec^{-1} keV^{-1}. The time resolution is 10.24 seconds.

++ γ_m is the spectral index at the time of 20 keV peak flux.

$\bar{\gamma}$ is the average spectral index.

+++ See Table II in Datlowe (1974b).

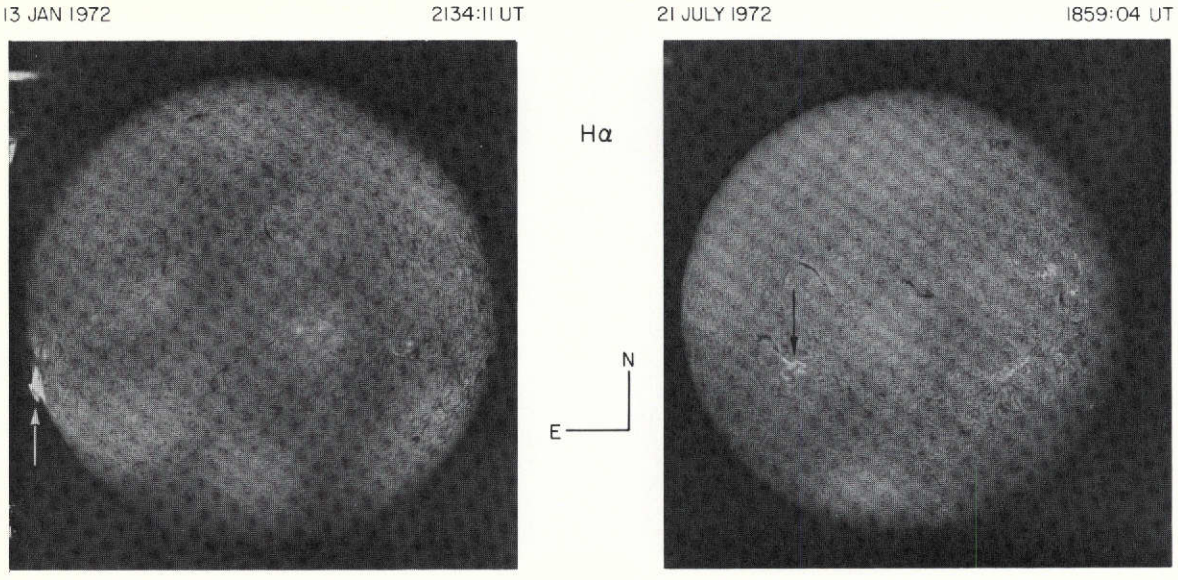

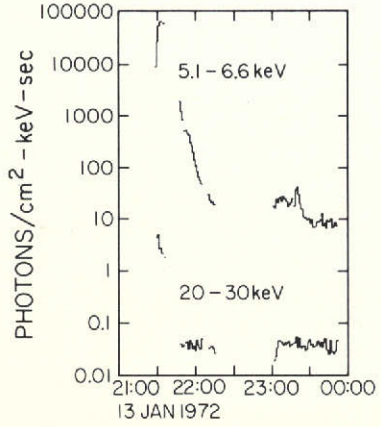

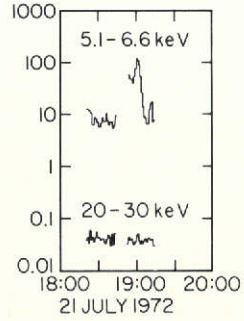

61.44 SECOND AVERAGE

UCSD OSO-7
X-RAY EXPERIMENT

Figure 1.

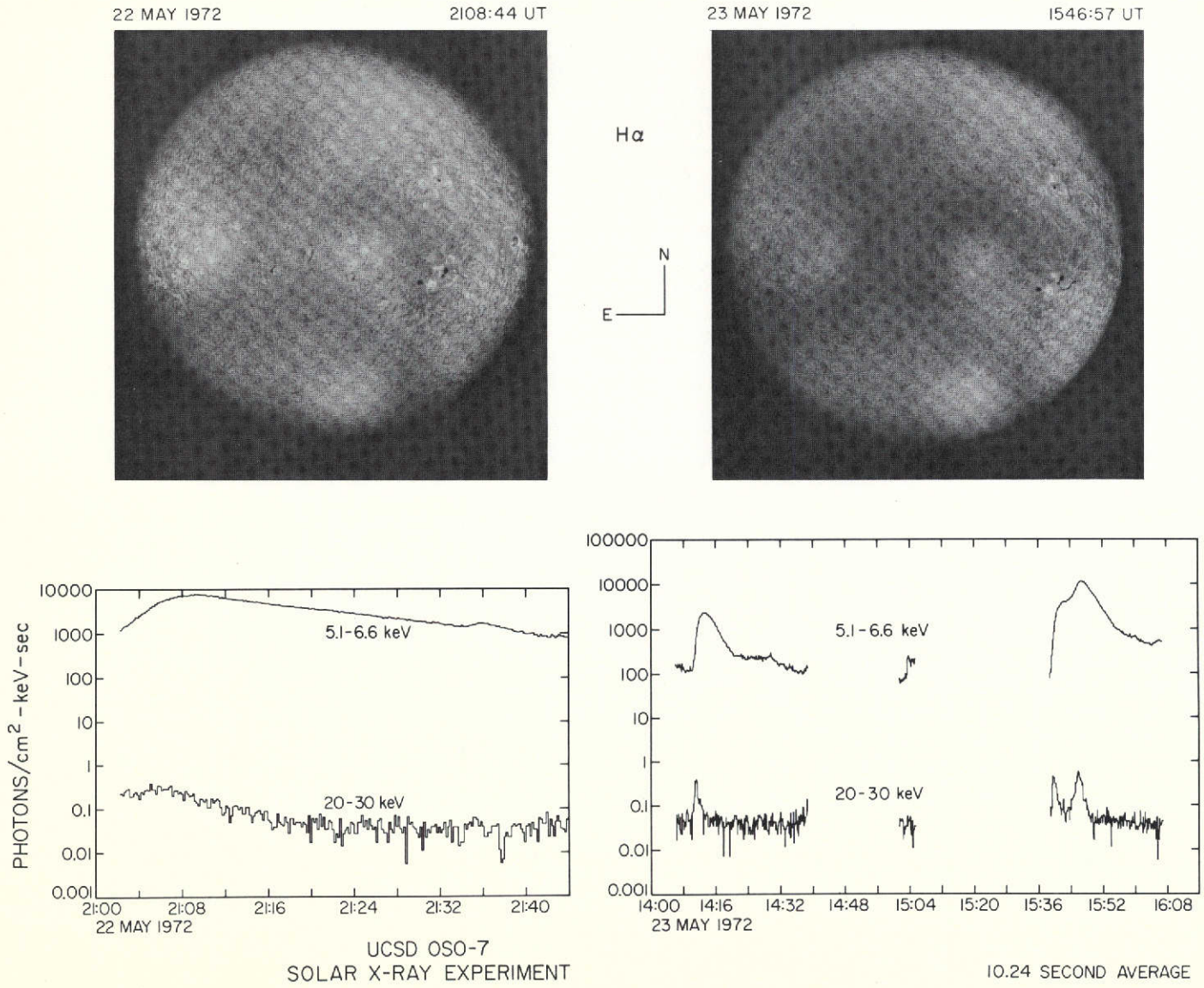
22 MAY 1972
2108:44 UT
23 MAY 1972
1546:57 UT
Hα
N
E
PHOTONS/cm² - keV - sec
10000
1000
100
10
1
0.1
0.01
0.001
5.1-6.6 keV
20-30 keV
21:00
21:08
21:16
21:24
21:32
21:40
22 MAY 1972
100000
10000
1000
100
10
1
0.1
0.01
0.001
5.1-6.6 keV
20-30 keV
14:00
14:16
14:32
14:48
15:04
15:20
15:36
15:52
16:08
23 MAY 1972
UCSD OSO-7
SOLAR X-RAY EXPERIMENT
10.24 SECOND AVERAGE

Figure 2.

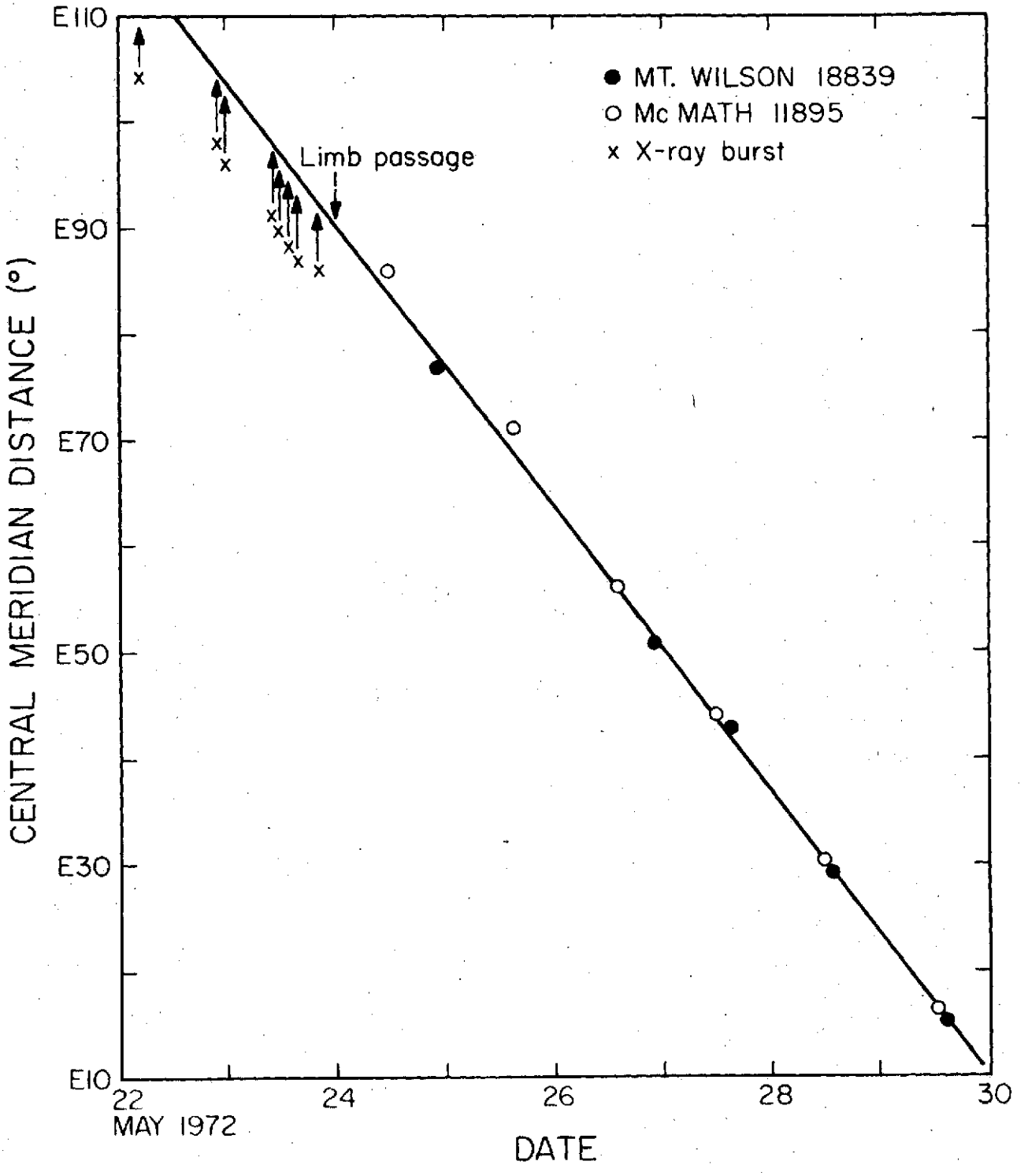
E110
E90
E70
E50
E30
E10
CENTRAL MERIDIAN DISTANCE (°)
MT. WILSON 18839
Mc MATH 11895
x X-ray burst
Limb passage
22
MAY 1972
24
26
28
30
DATE

Figure 3.

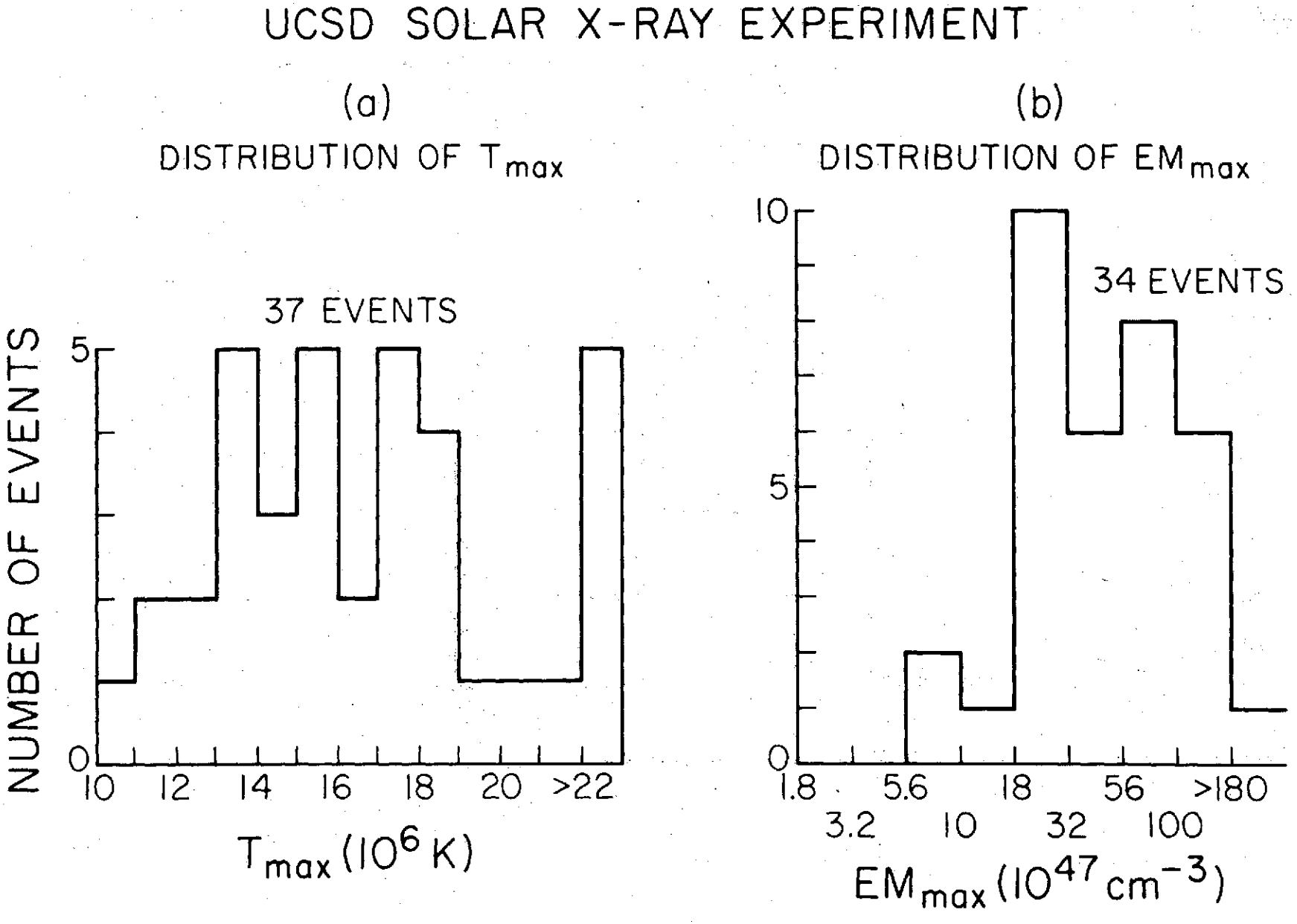
UCSD SOLAR X-RAY EXPERIMENT
(a)
DISTRIBUTION OF T_{max}
37 EVENTS
NUMBER OF EVENTS
0
5
10
12
14
16
18
20
>22
T_{max} (10^6 K)
(b)
DISTRIBUTION OF EM_{max}
34 EVENTS
0
5
10
1.8
3.2
5.6
10
18
32
56
100
>180
EM_{max} (10^{47} cm^{-3})

Figure 4 (a), (b)

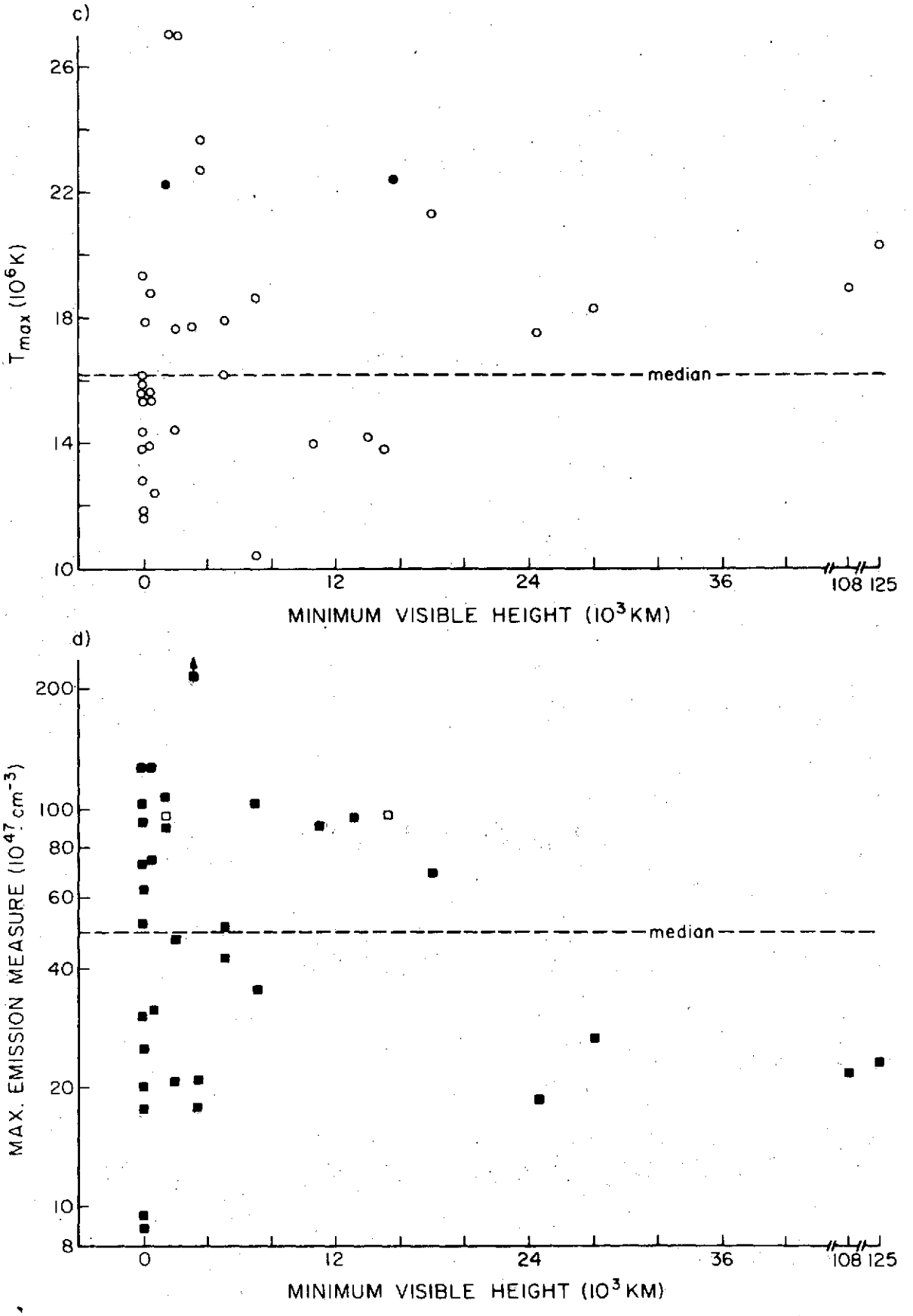
c)
26
22
18
14
10
T_{max} (10^6K)
median
0
12
24
36
108 125
MINIMUM VISIBLE HEIGHT (10^3KM)
d)
200
100
80
60
40
20
10
8
MAX. EMISSION MEASURE (10^{47} cm^{-3})
median
0
12
24
36
108 125
MINIMUM VISIBLE HEIGHT (10^3KM)

Figure 4 (c), (d)

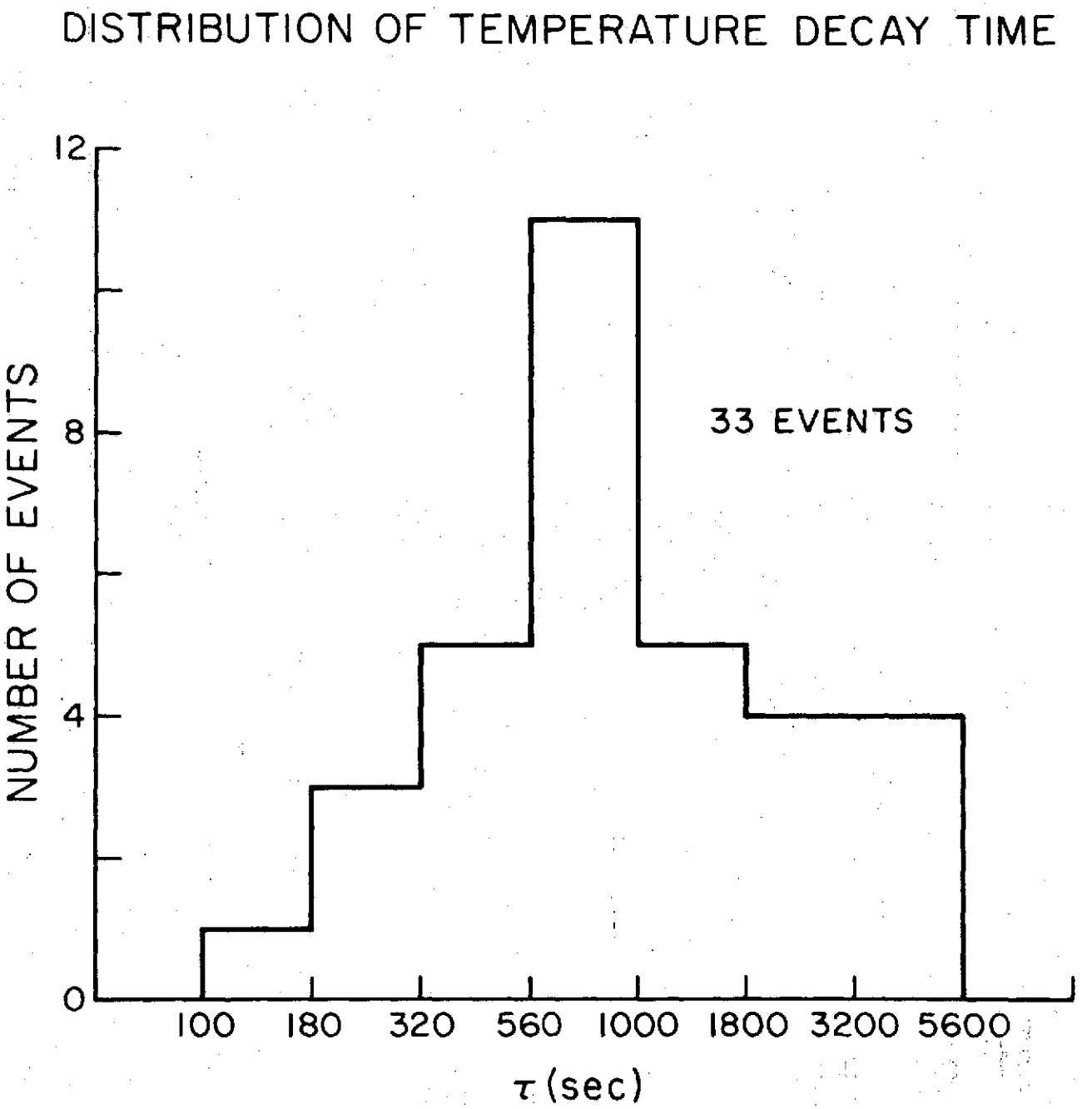
DISTRIBUTION OF TEMPERATURE DECAY TIME
NUMBER OF EVENTS
12
8
4
0
33 EVENTS
100
180
320
560
1000
1800
3200
5600
τ (sec)

Figure 5.

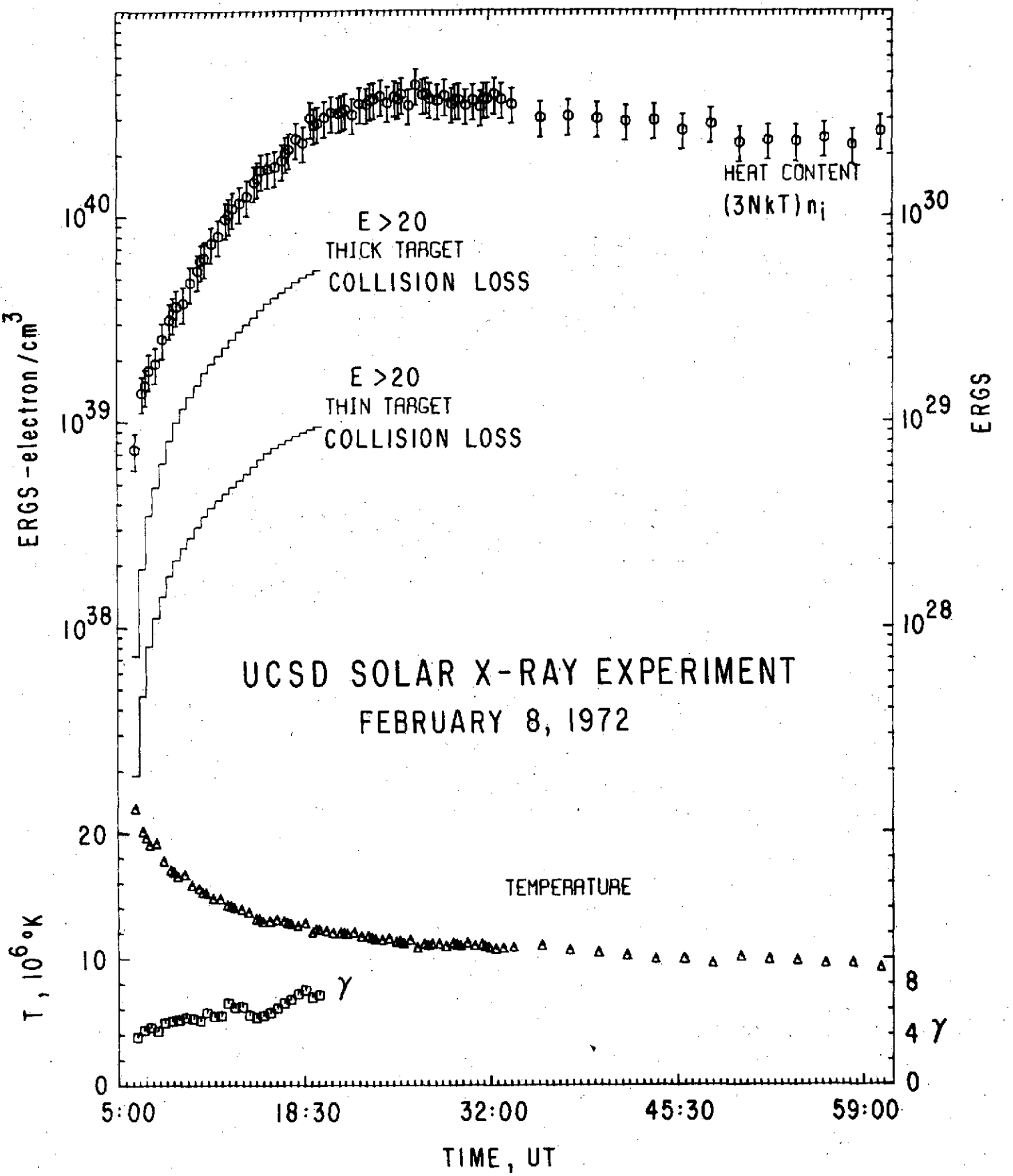
HEAT CONTENT
(3NkT)n_i
E>20
THICK TARGET
COLLISION LOSS
E>20
THIN TARGET
COLLISION LOSS
UCSD SOLAR X-RAY EXPERIMENT
FEBRUARY 8, 1972
TEMPERATURE
γ
ERGS-electron/cm^3
ERGS
T, 10^6 °K
TIME, UT
10^40
10^39
10^38
10^30
10^29
10^28
20
10
0
8
4
5:00
18:30
32:00
45:30
59:00

Figure 6.

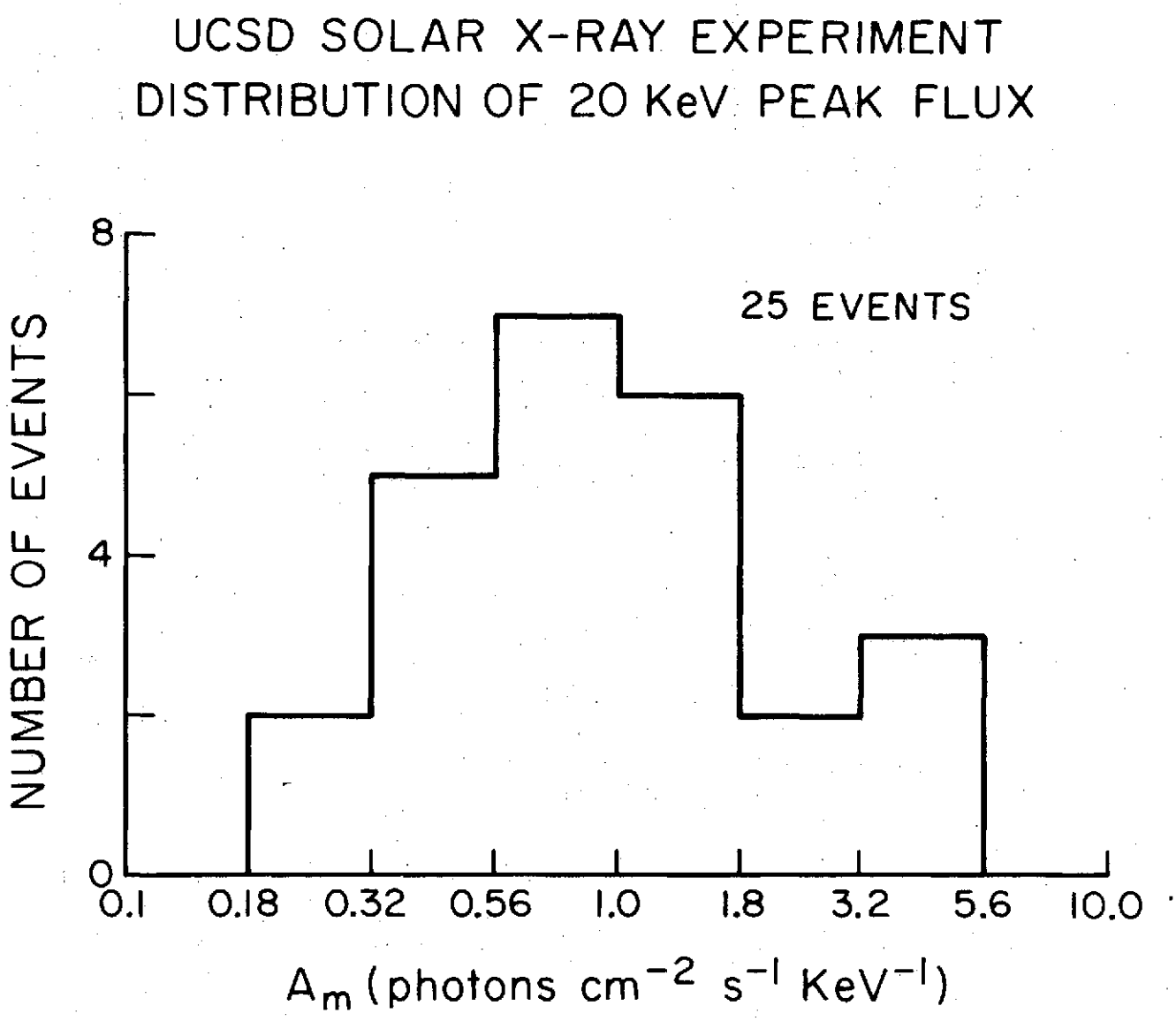
UCSD SOLAR X-RAY EXPERIMENT
DISTRIBUTION OF 20 KeV PEAK FLUX
NUMBER OF EVENTS
8
4
0
25 EVENTS
0.1
0.18
0.32
0.56
1.0
1.8
3.2
5.6
10.0
A_m (photons cm^{-2} s^{-1} KeV^{-1})

Figure 7.

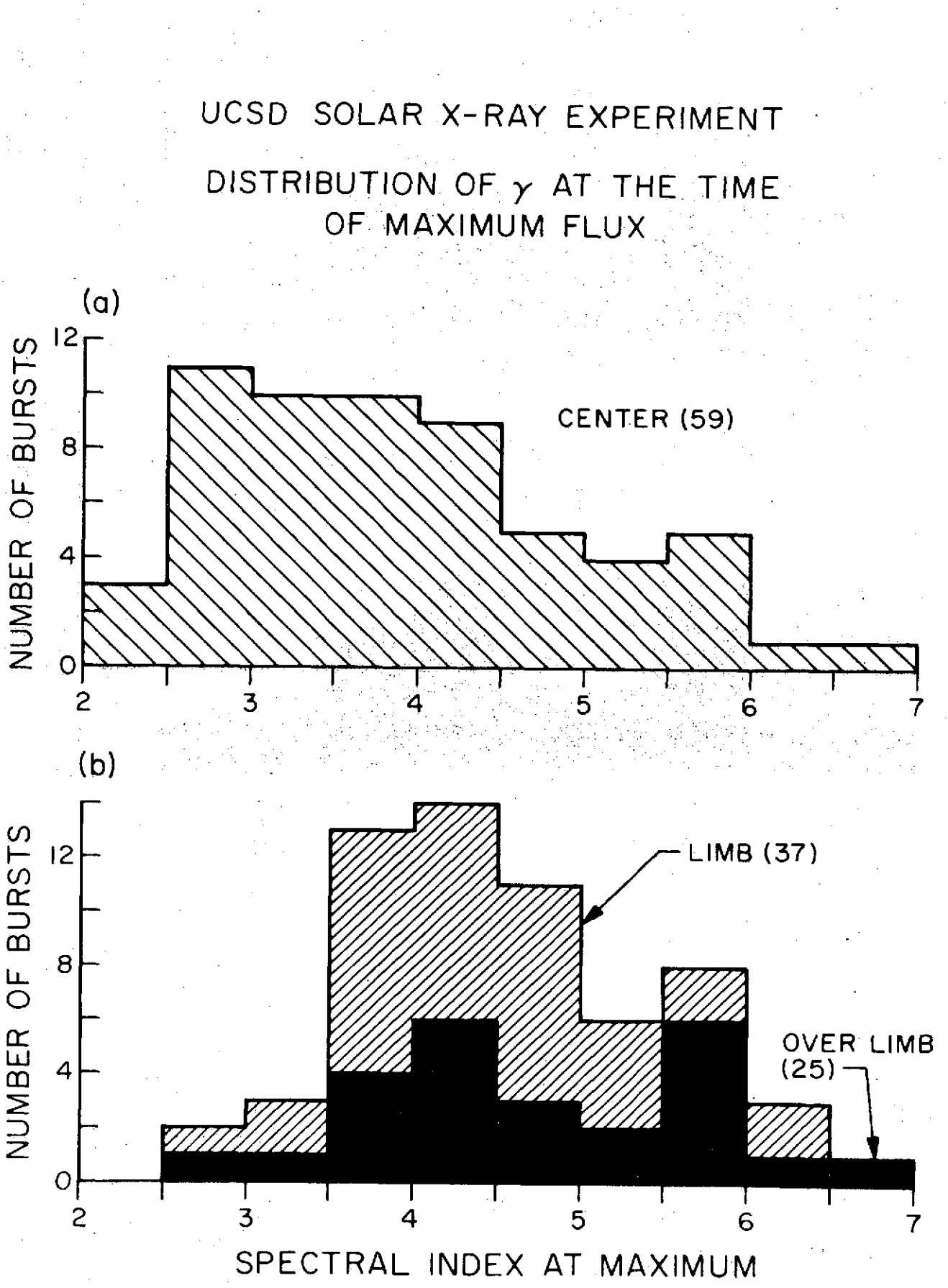
UCSD SOLAR X-RAY EXPERIMENT
DISTRIBUTION OF γ AT THE TIME OF MAXIMUM FLUX
(a)
NUMBER OF BURSTS
12
8
4
0
CENTER (59)
2
3
4
5
6
7
(b)
NUMBER OF BURSTS
12
8
4
0
LIMB (37)
OVER LIMB (25)
2
3
4
5
6
7
SPECTRAL INDEX AT MAXIMUM

Figure 8

Table A

X-ray bursts from flares near and behind the limb

	Date	Time UT)	Fluxes (photons $cm^{-2} s^{-1} keV^{-1}$) 5.1-6.6 keV	20-30 keV	Candidate region (Mt Wilson)	Longitude (°)	Minimum visible height (km)	
1971	28 Oct	0632	2×10^3	0.31	18594	W88	0	
	28 Oct	2130	3×10^3	0.15	18594	W97	5000	
	10 Nov	1057	5×10^3	0.21	18622	E122	125000	
	10 Nov	1340	5.2×10^3	0.62	18622	E120	108000	
	19 Nov	1400	$>10^4$	0.67	18633-34	E114	66000	
	20 Nov	0720	2.6×10^4	7.24	18633-34	E104	21000	
	31 Dec	0110	7×10^3	0.44	18665	W89	0	double burst
	31 Dec	0215	1.4×10^3	0.30	18665	W90	0	double burst
	31 Dec	0700	0.6×10^3	0.12	18665	W92	400	
	31 Dec	1355	1.6×10^3	0.17	18665	W95	2000	
1972	01 Jan	1008	1.8×10^3	0.17	18665	W105	24500	
	01 Jan	1230	1.8×10^3	0.22	18665	W106	28000	
	27 Jan	1720	0.5×10^3	--	18683-84	W94	1400	
	28 Jan	0400	9×10^3	0.21	18683-84	W100	10600	
	30 Jan	1520	7.5×10^3	0.38	18696	W89	0	
	30 Jan	1805	2×10^3	0.30	18696	W91	100	
	08 Feb	0715	7.6×10^3	0.52	18698 18715-19	W102 E94	15500 1400	

08 Feb	1950	2.2×10^3	0.24	18698 18715-19	W110 E90	44500 0
15 Feb	1633	5.3×10^3	0.44	18732	E95	2000
29 Feb	1515	$>5 \times 10^4$	1.76	18748	E94-96	1400-3550
13 May	0000	$>10^3$	--	18834	E100	10600
13 May	0130	$>10^3$	--	18834	E99	8500
13 May	0210	1.7×10^3	--	18834	E98	7000
13 May	1357	2.2×10^4	0.80	18834	E92	400
22 May	0530	$\sim 10^3$	--	18839	E113	60000
22 May	2109	7.7×10^3	0.39	18839	E103	18000
22-23 May	2300	9.4×10^3	0.21	18839	E102	15000
23 May	1120	4.9×10^3	1.77	18839	E97	5000
23 May	1412	2.4×10^3	0.40	18839	E96	3500
23 May	1546	1.1×10^4	0.60	18839	E94	1500 double burst
23 May	2021	2.2×10^3	--	18839	E93	700
15 Jul	0255	2.1×10^4	2.18	18903	W92	400
15 Jul	0630	0.95×10^3	--	18903	W94	1400
11 Aug	0010	8.1×10^3	0.50	18935	W83	0
11 Aug	0810	1.7×10^3	0.18	18935	W87	0
11 Aug	1100	0.9×10^3	0.35	18935	W90	0
11 Aug	2325	3.5×10^3	0.95	18935	W96	3500
12 Aug	1440	$>3 \times 10^4$	>0.50	18935	W105	24500
12 Aug	2045	$>6 \times 10^3$	--	18935	W109	40000

26 Aug	0343	8.7×10^3	1.14	18962	E98	7000
26 Aug	0832	1.0×10^3	0.17	18962	E95	2100
26 Aug	2225	8.3×10^3	0.65	18962	E88	0
27 Aug	0254	1.2×10^4	0.47	18962	E85	0
18 Sep	2200	1.4×10^3	--	18992	E97	5000
22 Oct	0942	3×10^3	0.25	19026	E96	3500
22 Oct	1050	2×10^4	2.66	19026	E95	2100
22 Oct	1105	7×10^3	0.20	19026	E95	2100
22 Oct	1230	1.0×10^4	0.87	19026	E94	1400
22 Oct	2000	3.8×10^3	0.21	19026	E90	0
23 Oct	0204	2.7×10^3	1.69	19026	E86	0
23 Oct	0220	7.9×10^3	0.33	19026	E86	0

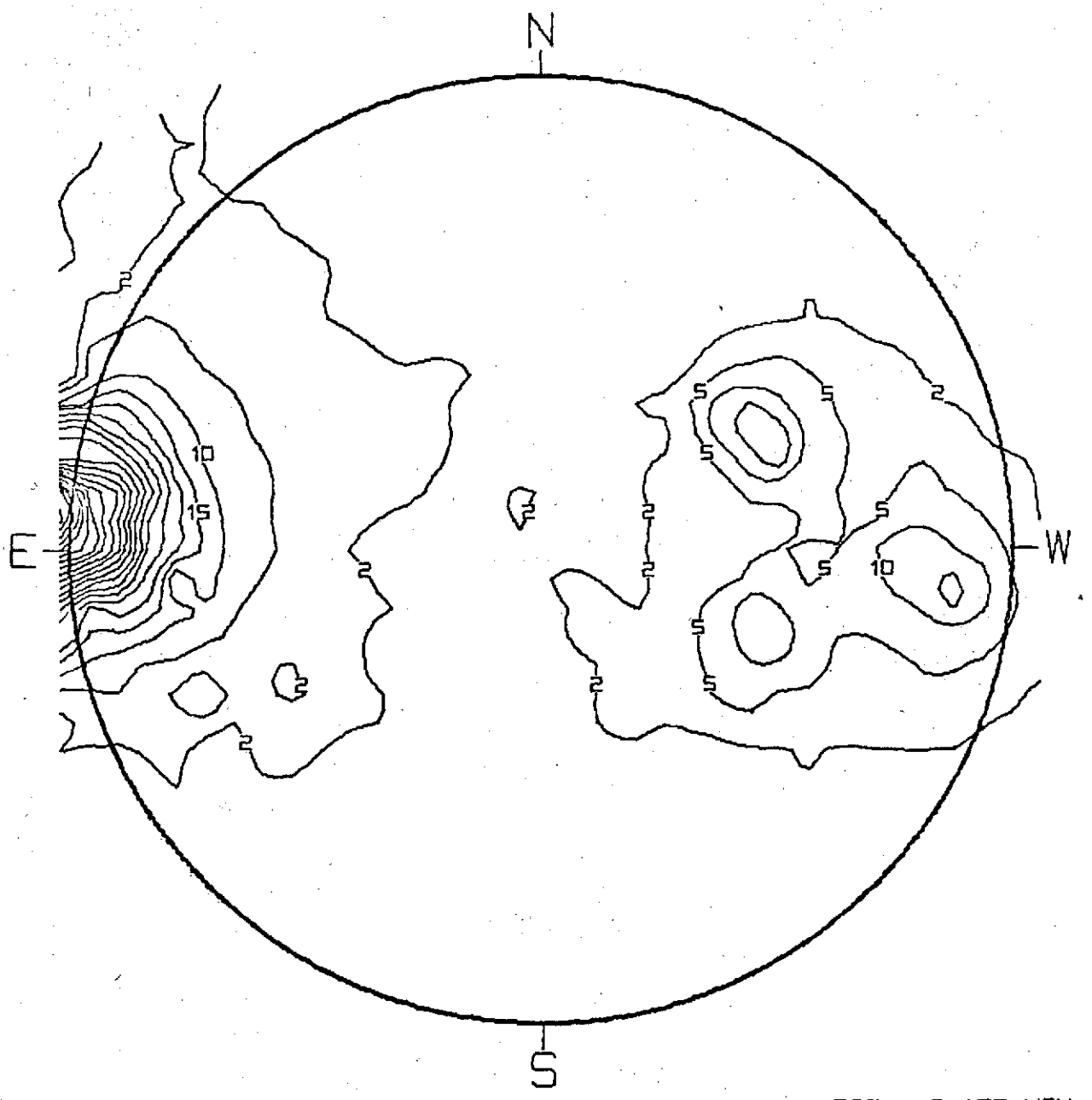

23 MAY 72

Figure A.

Table B

Physical parameters of X-ray bursts from behind the limb flares

OSO-7 orbit	Date	Time	Spectrum	T_{max} $\times 10^6$ K	EM_{max} $\times 10^{47}$ cm^{-3}	γ_m	γ(min)	A (20 keV)
	1971							
446	Oct. 28	0632	Hard	13.88	30	3.94	3.61	0.48
456	Oct. 28	2130	Soft	16.12	41			
649	Nov. 10	1054	Soft	20.22	23			
651	Nov. 10	1340	Hard	18.97	22	4.39	4.01	1.05
1430 i	Dec. 31	0103	Hard	15.59	10	3.62	2.68	0.18
1430 ii	Dec. 31	0110	Hard	14.35	93	4.62	4.62	0.75
1431 i	Dec. 31	0210	Hard	15.84	9	4.33	3.01	0.25
1431 ii	Dec. 31	0217	Hard	13.96	20	3.57	3.53	0.40
1438	Dec. 31	1354	Soft	14.47	20			
	1972							
1451	Jan. 01	1003	Soft	17.49	18			
1453	Jan. 01	1230	Hard	18.22	27	4.9		0.34
1865	Jan. 28	0400	Soft	13.91	90			
1903	Jan. 30	1520	Hard	15.35	74	4.24	4.24	0.77
1905	Jan. 30	1805	Hard	17.93	--	4.31	3.44	0.54
2037	Feb. 08	0715	Hard	22.37	97	5.51	3.83	1.07
2151	Feb. 15	1633	Hard	17.62	47	5.30	2.98	1.03
2367	Feb. 29	1515	Hard	17.69	>220	5.69	4.04	4.66
3503	May 13	0210	Soft	10.44	35			
3512	May 13	1357	Soft	15.64	129			

3656	May 22	2109	Hard	21.26	70	5.43	4.19	0.77
3657	May 22-23	2300	Hard	14.20	99	4.98	4.45	0.46
3665	May 23	1120	Hard	17.94	51	4.16	3.92	3.74
3667	May 23	1412	Hard	23.63	21	3.95	3.36	0.72
3668 i	May 23	1540	Hard	27.07	>115	3.45	3.32	0.75
3668 ii	May 23	1546	Hard	27.07	92	5.96	5.96	1.67
3671	May 23	2021	Soft	12.36	32			
4900	Aug. 11	0010	Hard	11.80	129	5.80	5.78	0.95
4905	Aug. 11	0810	Soft	16.11	18			
4915	Aug. 11	2325	Hard	22.72	19	4.17	3.92	1.62
5135	Aug. 26	0343	Soft	18.53	106			
5147	Aug. 26	2225	Soft	11.67	---			
5150	Aug. 27	0254	Hard	19.32	106	6.57	3.76	1.01
6026	Oct. 22	1051	Hard	14.58	65	5.35		5.42
6027	Oct. 22	1230	Hard	18.79	109	6.08	5.56	1.88
6032	Oct. 22	2000	Soft	12.78	52			
6036 i	Oct. 23	0203	Hard	13.56	25	2.60		2.33
6036 ii	Oct. 23	0216	Hard	15.29	74	7.27		0.70

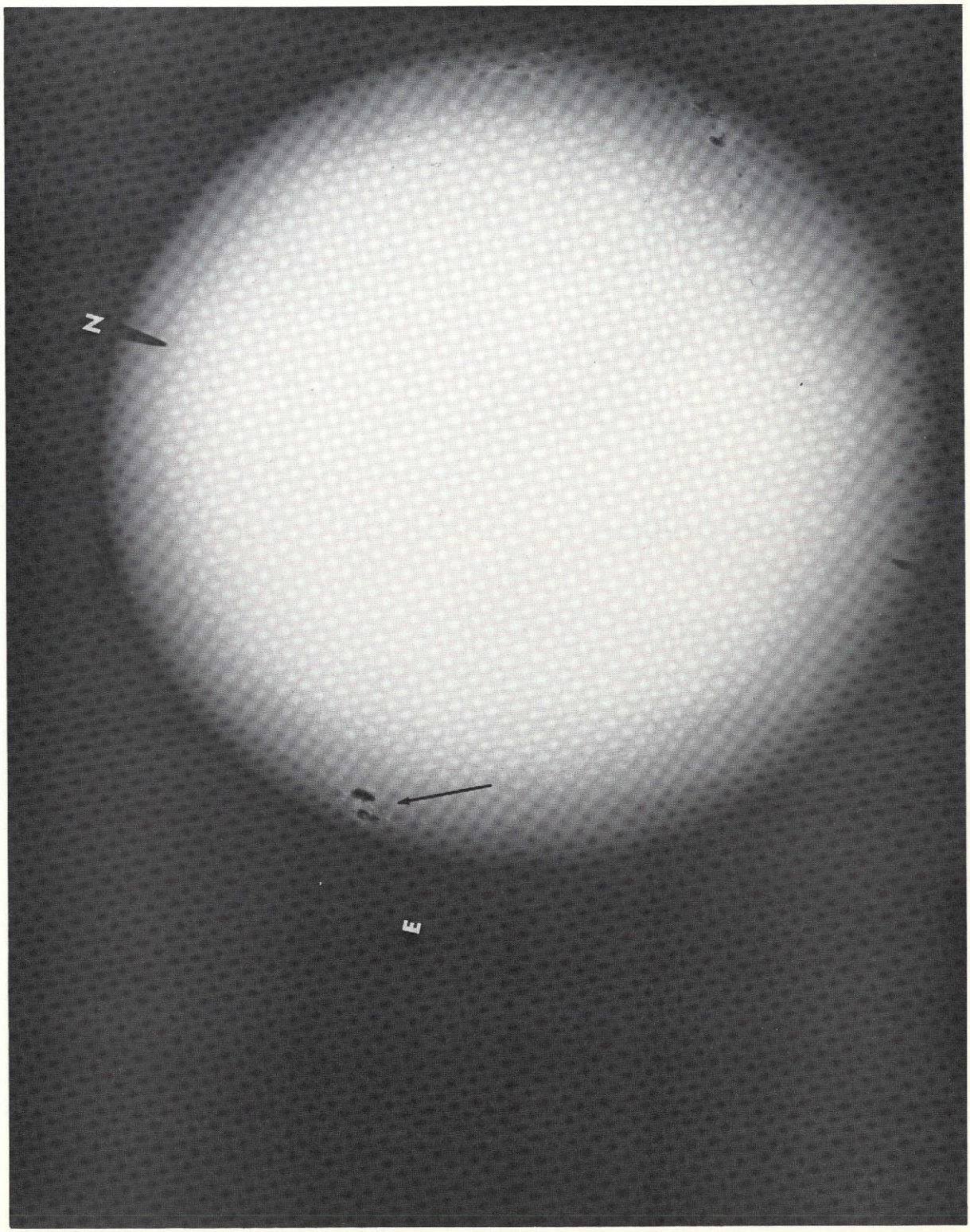

Figure B.